Polymerization of Ethylene Catalyzed by a Nickel(+2) Anilinotropone-Based Catalyst: DFT and Stochastic Studies on the Elementary Reactions and the Mechanism of Polyethylene Branching

Artur Michalak*,†,‡ and Tom Ziegler†

Department of Chemistry, University of Calgary, University Drive 2500, Calgary, Alberta, Canada T2N 1N4, and Department of Theoretical Chemistry, Faculty of Chemistry, Jagiellonian University, R. Ingardena 3, 30-060 Cracow, Poland

Received January 30, 2003

The results of combined DFT/stochastic studies on the mechanism of ethylene polymerization catalyzed by a neutral Ni-anilinotropone complex are presented. The generation of active species by phosphine dissociation and chain propagation and chain isomerization reactions have been investigated. The alternative methyl acrylate binding modes have also been studied. Further, the DFT-calculated energetics of the elementary reactions have been used to model the influence of the reaction conditions (*T*, *P*) on the branching/microstructure of polyethylenes produced in this process. The model and real catalysts (N^O−Ni; N^O = −N(Ar)−(C_7H_5)−O−, with Ar = H and Ar = C_6H_3(*i*-Pr)$_2$, respectively) have been considered to account for the electronic and steric effects. The presence of two *cis*/*trans* isomers for all the reactions has been considered. The results indicate that for the real anilinotropone catalyst the phosphine dissocciation is less endothermic (22 kcal/mol) than for the corresponding salicylaldiminato system (29 kcal/mol). The more branched alkyl agostic complexes are found to be more stable than the less branched and the linear isomers, while the stability order for the olefin-alkyl complexes is opposite. Thus, the stability of the alkyl complexes shifts the equilibrium toward formation of the branched species, while the stability of ethylene complexes favors formation of linear structures. The DFT results show that the energetically preferred pathways for the chain propagation and isomerization reactions start from the higher energy *cis*/*trans* isomers (with the alkyl positioned *trans* to the N atom on the catalyst). The preferred isomerization reactions have very low barriers (2.4−4.5 kcal/mol for different alkyl species). Along these pathways the unusually stable olefin-hydride complexes are formed, some of them being more stable (by 1.5−3 kcal/mol) than the alkyl agostic complexes. The results of the calculations for the methyl acrylate complexes confirm the high tolerance of the anilinotropone catalyst toward polar groups: the π-complexes are more stable by 8−13 kcal/mol than the systems with the acrylate molecule bound by its carbonyl oxygen. This functional group tolerance is larger than for the Grubbs catalyst. Also, the acrylate π-complexation energies are less affected by the steric bulk than in the case of salicylamidato catalysts and the diimine catalysts. Finally, the results of the stochastic simulations quantitatively reproduce the experimental trends in the temperature and pressure dependence of the average number of branches. In addition, the stochastic simulations provide detailed information about the variations in the topology of polyethylenes produced under different conditions.

Introduction

There has been an increasing interest in employing late transition metal-based complexes as α-olefin polymerization catalysts.[1,2] The late-metal complexes are less electrophilic than the early-metal system, thus providing the prospect for copolymerization of nonpolar α-olefins with polar monomers.[3] The first successful example[4,5] of a system capable of copolymerizing ethylene with acrylates was Pd-diimine complexes.[1,6,7] The Ni- and Pd-diimine catalysts were also shown to produce polymers with unique achitectures; the branching and topology of polyolefins obtained with these catalysts can

* Corresponding author. E-mail: michalak@chemia.uj.edu.pl.
† University of Calgary.
‡ Jagiellonian University.

(1) Ittel, S. D.; Johnson, L. K.; Brookhart, M. *Chem. Rev.* **2000**, *100*, 1169, and references therein.
(2) Britovsek, G. J. P.; Gibson, V. C.; Wass, D. F. *Angew. Chem., Int. Ed.* **1999**, *38*, 428, and references therein.
(3) Boffa, L. S.; Novak, B. M. *Chem. Rev.* **2000**, *100*, 1479, and references therein.
(4) Johnson, L. K.; Mecking, S.; Brookhart, M. *J. Am. Chem. Soc.* **1996**, *118*, 267.
(5) Mecking, S.; Johnson, L. K.; Wang, L.; Brookhart, M. *J. Am. Chem. Soc.* **1998**, *120*, 888.
(6) Johnson, L. K.; Killian, C. M.; Brookhart, M. *J. Am. Chem. Soc.* **1995**, *117*, 6414.
(7) Killian, C. M.; Tempel, D. J.; Johnson, L. K.; Brookhart, M. *J. Am. Chem. Soc.* **1996**, *118*, 11664.

10.1021/om030072+ CCC: $25.00
Publication on Web 04/04/2003

Scheme 1. Ni-Based Anilinotropone (A) and Salicylaldiminato (B) Catalyst

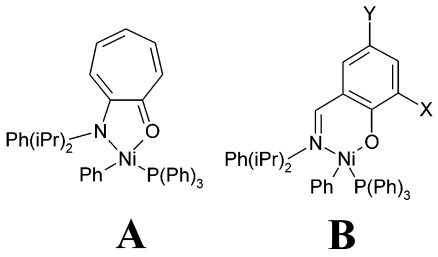

be controlled by the structure of the catalyst as well as by the reaction conditions (pressure and temperature).[1,8−11]

Most of the polymerization processes carried out by single-site catalysts involve *cationic* active species generated from the precatalyst by activation with a cocatalyst. The role of a cocatalyst during the polymerization process is still not completely understood and is a subject of extensive experimental[12] and theoretical[13] investigations. Therefore, there is an interest in developing *neutral* late transition metal systems that do not require a cocatalyst. As the first example, the neutral Ni-salicylaldimidato catalysts (**B** in Scheme 1) by Grubbs et al.[14,15] are characterized by activities comparable with the best cationic systems. The neutral catalysts are less electrophilic than the cationic species and therefore can potentially lead to a successful polar copolymerization.

Recently, a new neutral Ni-based polymerization catalyst has been reported by Hicks and Brookhart.[16] The anilinotropone-based complex (**A** in Scheme 1) is capable of polymerizing ethylene with high turnover frequency and of producing polymers with a wide range of branching numbers by changes in the reaction conditions (temperature and pressure). It is also very tolerant toward polar additives and insensitive to PPh_3.[16]

Quantum chemistry has established itself as a valuable tool for understanding the mechanistic details of the polymerization processes.[17,18] However, modeling the polymer branching/microstructure is beyond the practical abilities of ab initio calculations. Here, use of statistical methods is required. Recently,[19] we proposed a "mesoscopic" model for stochastic (Monte Carlo) simulations of the polymer growth that makes it possible to investigate the influence of the catalyst and the reaction condition on the polymer branching/microstructure directly from the results of quantum calculations.

Scheme 2. Complexes Studied in the Present Work

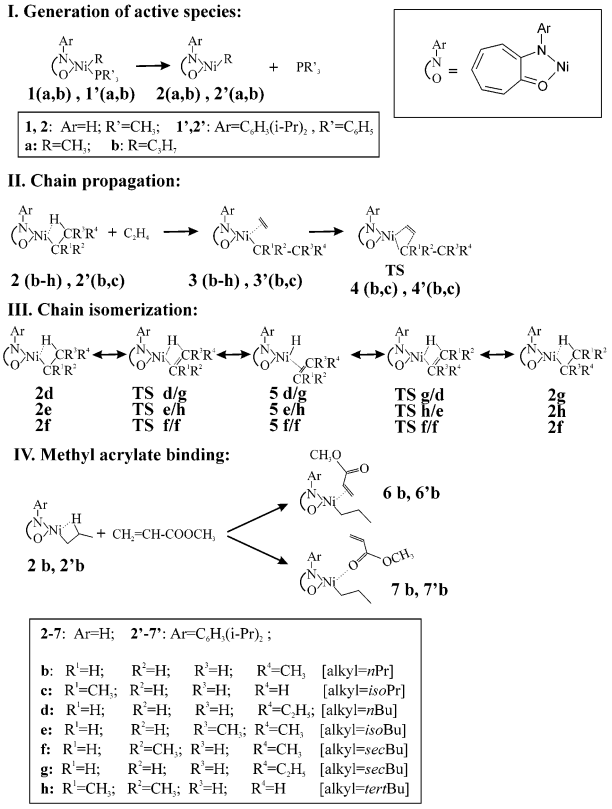

In the present study we report results from extensive theoretical studies on the mechanism of ethylene polymerization catalyzed by Ni-anilinotropone systems and the factors controlling the polymer branching/topology. We also address the issue of polar copolymerization by investigating the methyl acrylate binding modes. We employ a combined DFT/stochastic approach that allows us to investigate the details of the elementary reaction in the process as well as their influence on the polymer branching/topology. For the first time in the literature we reproduce semiquantitatively the experimental temperature and pressure dependence of the branching numbers directly from first-principles calculations. We also predict the variation in the polymer topology under different reaction conditions (*T* and *P*). Up to date, no mechanistic details, neither experimental nor theoretical, of the processes catalyzed by this system have been published. The communication by Hicks and Brookhart[16] reports the pressure and temperature dependence of the average number of branches; however, the topology of the polymers has not been characterized. No polar copolymerization activity of this promising system has been reported yet.

Computational Details and the Model Systems

The molecular systems studied in the present work are shown in Scheme 2. Two models for the catalyst, N^O−Ni, have been used: a generic complex with N^O = −NH−(C_7H_5)−O−, in which the bulky substituents on the nitrogen atoms

(8) Guan, Z.; Cotts, P. M.; McCord, E. F.; McLain, S. J. *Science* **1999**, 283, 2059.
(9) Cotts, P. M.; Guan, Z.; McCord, E. F.; McLain, S. J. *Macromolecules* **2000**, *33*, 6945.
(10) Gates, D. P.; et al. *Macromolecules* **2000**, *33*, 2320.
(11) McCord, E. F.; et al. *Macromolecules* **2001**, *34*, 362.
(12) Chen, E. Y. X.; Marks, T. J. *Chem. Rev.* **2000**, *100*, 1391.
(13) (a) Klesing, A.; Bettonville, S. *Phys. Chem. Chem. Phys.* **1999**, *1*, 2373−2377. (b) Chan, M. S. W.; Vanka, K.; Pye, C. C.; Ziegler, T. *Organometallics* **1999**, *18*, 4624. (c) Lanza, G.; Fragala, I. L.; Marks, T. J. *J. Am. Chem. Soc.* **1998**, *120*, 8257. (d) Lanza, G.; Fragala, I. L. *Top. Catal.* **1999**, *7*, 45. (e) Nifant'ev, I. E.; Ustynyuk, L. Y.; Laikov, D. N. *Organometallics* **2001**, 20, 5375. (f) Vanka, K.; Chan, M. S. W.; Pye, C. C.; Ziegler, T. *Organometallics* **2000**, *19*, 1841. (g) Chan, M. S. W.; Ziegler, T. *Organometallics* **2000**, *19*, 5182. (h) Vanka, K.; Ziegler, T. *Organometallics* **2001**, *20*, 905. (i) Xu, Z.; Vanka, K.; Firman, T.; Michalak, A.; Zurek, E.; Zhu, C.; Ziegler, T. *Organometallics* **2002**, *21*, 2444. (j) Lanza, G.; Fragala, I. L.; Marks, T. J. *J. Am. Chem. Soc.* **2000**, *122*, 12764.
(14) Wang, C.; Friedrich, S.; Younkin, T. R.; Li, R. T.; Grubbs, R. H.; Bansleben, D. A.; Day, M. W. *Organometallics* **1998**, *17*, 3149.
(15) Younkin, T. R.; Connor, E. F.; Henderson, J. I.; Friedrich, S. K.; Grubbs, R. H.; Bansleben, D. A. *Science* **2000**, *287*, 460.
(16) Hicks, F. A.; Brookhart, M. *Organometallics* **2001**, *20*, 3217.
(17) Rappe, A. K.; Skiff, W. M.; Casewit, C. J. *Chem. Rev.* **2000**, *100*, 1435, and references therein.
(18) Angermund, K.; Fink, G.; Jensen, V. R.; Kleinschmidt, R. *Chem. Rev.* **2000**, *100*, 1457, and references therein.
(19) Michalak, A.; Ziegler, T. *J. Am. Chem. Soc.* **2002**, *124*, 7519.

were replaced by hydrogen atoms, and a "real" catalyst with N^O = −N[C_6H_3(*i*-Pr)$_2$]−(C_7H_5)−O−. Throughout the article the structures involving the real catalyst will be numbered with primes. A comparison of the results for the generic and real catalysts allows us to understand the role of the electronic and steric effects.

The phosphine dissociation reaction (see Scheme 2, part I) was studied for both catalyst models; for the generic catalyst the trimethyl phosphine was used in structures **1** (**1a** and **1b**), while in the real system the triphenyl phosphine was considered in structures **1′** (**1′a** and **1′b**). In both cases methyl (structures **a**) and propyl (structures **b**) groups were used as models for the polymer chain.

For the chain propagation reactions (Scheme 2, part II) the calculations have been performed for the alkyl β-agostic complexes (**2**, **2′**), ethylene π-complexes (**3**, **3′**), and the ethylene insertion transition states (**4**, **4′**). As we argued in the previous papers,[19−21] to model polyethylene branching one has to consider the isomeric complexes with primary, secondary, and tertiary carbons attached to the catalyst. Therefore, for the generic catalyst we considered the alkyl (**2**) and alkyl-olefin (**3**) complexes with propyls (complexes **b** and **c** for *n*- and *i*-Pr, respectively) and butyls (complexes **d**, **e**, **f/g**, and **h,** for *n*-, *iso*-, *sec*-, and *tert*-Bu, respectively; note the presence of two isomers, **f** and **g**, for *sec*-Bu β-agostic complexes). For the real catalyst, calculations have been performed for the alkyl (**2′**) and alkyl-olefin (**3′**) complexes with the *n*- (structures **b**) and *iso*-propyl (structures **c**) groups at the catalyst. For both the generic and the real catalyst, the ethylene insertion TS (**4**, **4′**) has been optimized for the complexes with *n*- and *iso*-Pr groups (structures **b** and **c**, respectively). We did not study insertions into the Ni−C bond involving the tertiary carbon atom since it may be expected that such reactions have much higher barriers due to steric congestion, as observed for other polymerization catalysts.[20] Neither have we performed calculations for the insertion products, as it is known that the ethylene insertion reactions are strongly exotermic and the relative stabilities of alternative insertion products (β-agostic complexes with isomeric alkyls) must be similar to the initial complexes **2**.

Use of the isomeric butyl groups as models for the polymer allows us to study the chain isomerization reactions involving the systems with primary, secondary, and tertiary carbons attached to the metal. We considered three isomerizations (see Scheme 2, part III): (1) **2d** ↔ **2g** (primary ↔ secondary); (2) **2e** ↔ **2h** (primary ↔ tertiary); (3) **2f** ↔ **2f** (secondary ↔ secondary). Without going to longer alkyl groups it is not possible to study isomerizations between the systems with secondary/tertiary and tertiary C at the metal (pentyl/hexyl groups would be required). However, the set of reactions considered here already provides information about the trends that can be "extrapolated" further. All the isomerization reactions proceed with the mechanism involving abstraction of the β-hydrogen, to form an olefin-hydride complex, and its reinsertion following the olefin rotation. In all the cases we performed calculations for the respective olefin hydride complexes (**5x/y**) and the pair of transition states "on both sides" (**TS x/y** and **TS y/x** for **x/y** = **d/g**, **e/h**, **f/f**). For the isomerization reactions (hydride complexes and the two TS) we use the generic catalyst only since it has been shown theoretically[20,21] and experimentally[22,23] that they are not affected by the presence of steric bulk on the catalyst even for more congested systems (α-diimine catalysts) than the catalyst studied in the present work. However, we would like to point out that we will discuss the effect of the steric bulk on the stability of alternative alkyl complexes (**2bc** vs **2′bc**).

Scheme 3. Example of the Two Alternative (*cis*/*trans*) Pathways for Ethylene Insertion

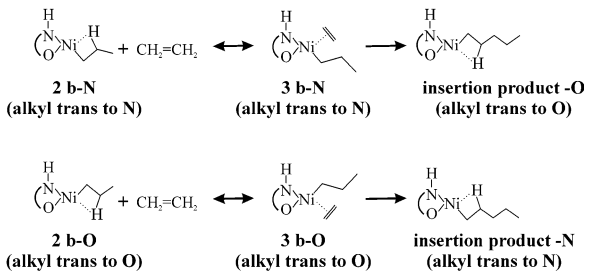

For the methyl acrylate complexes (Scheme 2, part IV) two binding modes were considered: π-complexes (**6b**, **6b′**) and O-complexes (**7b**, **7′b**). We use both the generic and the real catalyst in these calculations, as it has been shown for other catalysts that the complexation energies are strongly affected by the steric bulk.[21,24]

Finally, we would like to point out that due to the asymmetry of the catalyst, all the systems considered here have an additional two (*cis*/*trans*) isomers. Thus, all the reaction pathways are doubled. As an example, we illustrate this in Scheme 3 for the chain propagation reaction involving primary alkyl. In all the calculations presented here we considered both isomers for all the structures. We will refer to them by adding the **-N** and **-O** suffixes to the numbering presented in Scheme 2, depending on the position of the alkyl group (*trans* to N atom and *trans* to O atom, respectively). For example, for the alkyl complex **2b** the two structures are named **2b-N** and **2b-O**, respectively (Scheme 3).

All the DFT results were obtained from calculations based on the Becke−Perdew exchange−correlation functional,[25−27] using the Amsterdam Density Functional (ADF) program.[28−32] The standard double-ζ STO basis sets with one set of polarization functions were applied for H, C, N, P, and O atoms, while the standard triple-ζ basis sets were employed for the Ni atom.[33] The 1s electrons of C, N, and O as well as the 1s−2p electrons of P and Ni were treated as frozen core. Auxiliary s, p, d, f, and g STO functions,[34] centered on all nuclei, were used to fit the electron density and obtain accurate Coulomb and exchange potentials in each SCF cycle. The reported energy differences include a first-order scalar relativistic correction,[35−37] since it has been shown that such a relativistic approach is sufficient for 3d and 4d transition metal atoms.[38] The bond-order analysis for the alkyl complex **2b** and the corresponding complex with Grubbs catalyst (see Figure 1) was performed using the valence indices/bond-order analysis of Nalewajski et al.[39−42] This bond-order analysis has been chosen since it

(20) Michalak, A.; Ziegler, T. *Organometallics* **1999**, *18*, 3998.
(21) Michalak, A.; Ziegler, T. *Organometallics* **2000**, *19*, 1850.
(22) Shultz, L. H.; Brookhart, M. *Organometallics* **2001**, *20*, 3975.
(23) Shultz, L. H.; Tempel, D. J.; Brookhart, M. *J. Am. Chem. Soc.* **2001**, *123*, 11539.
(24) Michalak, A.; Ziegler, T. *Organometallics* **2001**, *20*, 1521.
(25) Becke, A. *Phys. Rev. A* **1988**, *38*, 3098.
(26) Perdew, J. P. *Phys. Rev. B* **1986**, *34*, 7406.
(27) Perdew, J. P. *Phys. Rev. B* **1986**, *33*, 8822.
(28) TeVelde, G.; Bickelhaupt, F. M.; Baerends, E. J.; Fonseca Guerra, C.; Van Gisbergen, S. J. A.; Snijders, J. G.; Ziegler, T *J. Comput. Chem.* **2001**, *22*, 931, and references therein.
(29) Baerends, E. J.; Ellis, D. E.; Ros, P. *Chem. Phys.* **1973**, *2*, 41.
(30) Boerrigter, P. M.; te Velde, G.; Baerends, E. J. *Int. J. Quantum Chem.* **1988**, *33*, 87.
(31) Versluis, L.; Ziegler, T. *J. Chem. Phys.* **1988**, *88*, 322.
(32) te Velde, G.; Baerends, E. J. *J. Comput. Phys.* **1992**, *99*, 84.
(33) Fonesca Geurra, C.; Visser, O.; Snijders, J. G.; te Velde, G.; Baerends, E. J. In *Methods and Techniques in Computational Chemistry METACC-95*; Clementi, E., Corongiu, G., Eds.; STEF: Cagliari, 1995.
(34) Snijders, J. G.; Baerends, E. J.; Vernoijs, P. *At. Nucl. Data Tables* **1982**, *26*, 483.
(35) Ziegler, T.; Tschinke, V.; Baerends, E. J.; Snijders, J. G.; Ravenek, W. *J. Phys. Chem.* **1989**, *93*, 3050.
(36) Snijders, J. G.; Baerends, E. J. *Mol. Phys.* **1978**, *36*, 1789.
(37) Snijders, J. G.; Baerends, E. J.; Ros, P. *Mol. Phys.* **1979**, *38*, 1909.
(38) Deng, L.; Ziegler, T.; Woo, T. K.; Margl, P.; Fan, T. *Organometallics* **1998**, *17*, 3240.

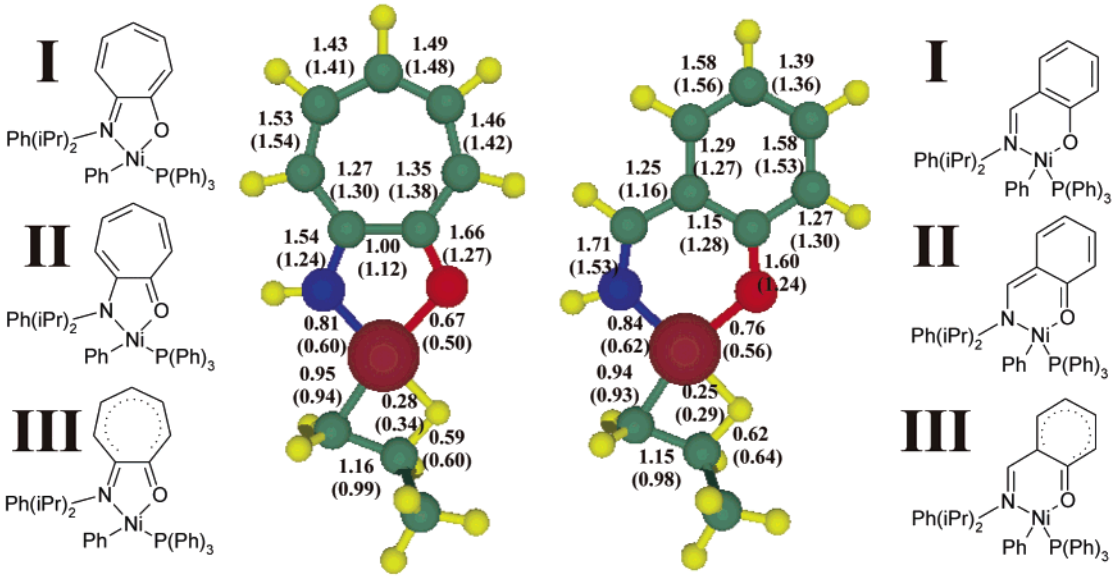

Figure 1. Results of the bond-order analysis for the alkyl β-agostic complexes with Ni-based anilinotropone (left) and salicylaldiminato (right) catalysts together with the alternative resonance structures of the catalysts. The values of the Nalewajski and Mayer (in parantheses) bond-order indices are presented.

includes both covalent and ionic indices, which seems to be especially important for the analysis of transition metal complexes. Also, the method is less basis set sensitive[41,42] than other schemes, as it is based on the well-defined atomic reference state. Since the approach of Nalewajski et al.[39−42] is relatively new and thus less popular than other bond-order indices, we compare the results with the Mayer bond-order analysis.[43,44]

Finally, stochastic simulations of the polymer growth and isomerization were performed using our own code and the method described in the recent paper.[19] This method uses as input data the energies/activation energies of the elementary reactions in the process and is based on the assumption that the relative probablilities of two reactive events (microscopic), π_i and π_j, are equal to their relative reaction rates (macroscopic), $\pi_i/\pi_j = r_i/r_j$; with the probability normalization constraint, $\sum_i \pi_i = 1$. Such an approach makes it possible to model the temperature and pressue effects. More specifically, the temperature dependence appears in the probabilities for all the events through the rate constants and equilibrium constants (Arrhenius/Eyring equations). The pressure affects directly the relative probabilities for unimolecular (isomerization)/bimolecular (ethylene capture + insertion) reactive events, and indirectly it influences all the probabilities because of probability normalization. Namely, the relative isomerization/insertion probability is given by[19]

$$\pi_{iso}/\pi_{ins} = r_{iso}/r_{ins} = k_{iso}/(k_{ins}\,Kp) \qquad (1)$$

where k_{iso} and k_{ins} are the insertion and the isomerization rate constants, K denotes the ethylene complexation equilibrium constant, and p stands for the olefin pressure. The more detailed description of the stochastic method was provided in ref 19. In the simulations performed in the present work the relative stabilities of alternative complexes and the energies of the elementary reactions obtained for the real catalyst were used as data for these simulations.

Results and Discussion

Resonance Structures of the Catalyst. Before we discuss the elementary reactions in the polymerization process we would like to briefly comment on the electronic structure of the catalyst. The salicylaldiminato (Grubbs) catalysts are usually drawn with the use of resonance structure **I** of Figure 1, i.e., with the C−N bond drawn as a double bond and C−O as a single. It has been argued by Hicks and Brookhart[16] on the basis of the bond lengths that for the anilinotropone catalyst the "opposite" structure should be used (resonance structure **II** of Figure 1), with the C−O double bond (see also Scheme 1). The results of the bond-order analysis for the alkyl complexes of both catalysts are presented in Figure 1; we present here values of the bond-order indices obtained by two independent approaches: from the Nalewajski[39−43] and the Mayer method.

The values of the bond-order indices obtained from both schemes partially confirm the suggestion of Hicks and Brookhart: for the anilitropone catalyst the C−O bond has slightly higher bond order (1.7 and 1.3, from the Nalewajski[39−42] and Mayer[43,44] method, respectively) than the C−N bond (1.5 and 1.2), while for the Grubbs catalyst the opposite trend is observed (1.6 and 1.2 vs 1.7 and 1.5); thus for the anilinotropone catalyst the resonance structure **II** has a slightly higher contribution. However, both of these bonds are "more double" than single in either of the complexes. This together with the bond polarization of the carbon rings suggests that the resonance structures **III** would be more appropriate in both cases. We would like to point out that in both structures the bridging C−C bonds have practically pure single-bond character. Also, it is worth mentioning that the bond-order analysis correctly describes agostic H−Ni interaction (ca. 0.3) and the corresponding C−H bond weakening (from ca. 0.9 to 0.6).

(39) Nalewajski, R. F.; Mrozek, J. *Int. J. Quantum Chem.* **1994**, *51*, 187.
(40) Nalewajski, R. F.; Mrozek, J.; Mazur, G. *Can. J. Chem.* **1996**, *74*, 1121.
(41) Nalewajski, R. F.; Mrozek, J.; Michalak, A. *Int. J. Quantum Chem.* **1997**, *61*, 589.
(42) Nalewajski, R. F.; Mrozek, J.; Michalak, A. *Polish. J. Chem.* **1998**, *72*, 1779.
(43) Mayer, I. *Chem. Phys Lett.* **1983**, *97*, 270.
(44) Mayer, I. *Chem. Phys Lett.* **1984**, *110*, 440.

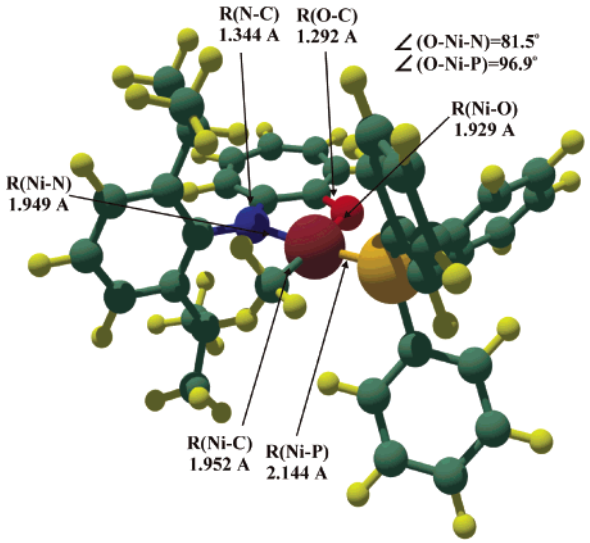

Figure 2. Calculated structure of the complex **1′a** (see Scheme 2).

Table 1. Enthalpy Change for the Phosphine Dissociation Reactions

reaction[a]	ΔH^b
1a → **2a** + $P(CH_3)_3$	53.4
1b → **2b** + $P(CH_3)_3$	30.4
1′a → **2′a** + $P(C_6H_5)_3$	38.2
1′b → **2′b** + $P(C_6H_5)_3$	22.0

[a] See Scheme 2. [b] In kcal/mol.

Finally, we would like to emphasize the fact that the bond orders obtained from the two methods are very close to each other for the backbone bonds, remote from the transition metal. The largest differences between the two approaches are observed within the catalyst ring comprising the metal atom. This is not surprising, as the Nalewajski bond-order indices include the ionic contributions, neglected in the Mayer scheme. These contributions are more important in the vicinity of the transition metal than for the typical "organic" bonds.

Generation of Active Site: Phosphine Dissociation. The generation of active species was modeled by the phosphine dissociation (Scheme 1, part I) from the generic (**1ab**) and real catalyst systems (**1′ab**). The optimized structure of the minimum energy conformer of the real catalyst presursor **1′a** with the methyl group at the metal is shown in Figure 2. The phosphine dissociation energies are collected in Table 1.

The results of the calculations show a very large difference between the dissociation energies for the system with methyl and propyl groups (**1a** vs **1b**, and **1′a** vs **1′b**). The dissociation energy of **1b** (30.4 kcal/mol) is lower by 23 kcal/mol than that of **1a** (53.4). For the real catalyst a much smaller, but still significant difference of 16 kcal/mol is observed (38.2 kcal/mol in **1′a** and 22 kcal/mol in **1′b**). This effect is a result of two factors: (i) destabilization of the structures **1b** and **1′b** due to the steric repulsion introduced by the propyl group, (ii) large stabilization of the dissociation product in **2b/ 2′b** compared to **2a/2′a** due to formation of the β-agostic metal−hydrogen bond. The results presented here demonstrate that the formation of the alkyl complexes with β-agostic bonds facilitates dissociation of phosphine during the polymerization process (compared to the initial stage when the polymer chain is not present yet).

Table 2. Relative Energies for the Alkyl β-Agostic and Ethylene π-Complexes Comprising Propyl and Butyl Groups

	relative energy[a]							
	β-agostic complexes[b]				ethylene π-complexes[b]			
alkyl	O-*trans*		N-*trans*		O-*trans*		N-*trans*	
				Propyl, Model Catalyst				
n-Pr	**2b-O**	0.89	**2b-N**	3.68	**3b-O**	0.06	**3b-N**	3.75
iso-Pr	**2c-O**	0.00	**2c-N**	2.34	**3c-O**	0.00	**3c-N**	2.79
				Propyl, Real Catalyst				
n-Pr	**2′b-O**	1.30	**2′b-N**	3.44	**3′b-O**	0.53	**3′b-N**	0.93
iso-Pr	**2′c-O**	0.00	**2′c-N**	1.85	**3′c-O**	5.08	**3′c-N**	0.00
				Butyl, Model Catalyst				
n-Bu	**2d-O**	2.85	**2d-N**	5.54	**3d-O**	0.00	**3d-N**	3.68
iso-Bu	**2e-O**	2.05	**2e-N**	4.52	**3e-O**	0.06	**3e-N**	4.40
sec-Bu	**2f-O**	2.07	**2f-N**	4.81	**3f-O**	0.56	**3f-N**	3.77
sec-Bu	**2g-O**	1.57	**2g-N**	3.56	**3g-O**	0.56	**3g-N**	3.77
tert-Bu	**2h-O**	0.00	**2h-N**	1.91	**3h-O**	4.23	**3h-N**	6.18

[a] With respect to the most stable isomer, in kcal/mol. [b] See Scheme 2.

A comparison of the present results with the previous calculations for the Grubbs catalyst[45] demonstrates that for the generic catalysts phosphine dissociation is easier for the salicylaldiminato system (27.3 kcal/mol) by ca. 3 kcal/mol than for the anilinotropone catalyst (30.4 kcal/mol for **1b**). However, in the case of the Grubbs catalyst practically no steric effect was observed[45] when introducing the $-Ph(i\text{-}Pr)_2$ group on the catalyst. For anilinotropone, steric effects are significant: dissociation energies are decreased by 15 kcal/mol (**1′a** vs **1a**) and 8 kcal/mol (**1′b** vs **1b**) for the systems with methyl and propyl groups, respectively. It should be emphasized, however, that in the systems **1′a** and **1′b** the "real" triphenyl phosphine was used in the present studies. The $P(C_6H_5)_3$ ligand can be expected to introduce a substantial steric congestion compared to $P(CH_3)_3$. Finally, the phosphine dissociation energy calculated for the system **1′b** (22 kcal/mol) is lower than all the energies calculated for Grubbs catalysts with different substituents (23.7−27.9 kcal/mol). When comparing our results with the results previously published[45] for the Grubbs system, one should remember, however, that the QM/MM approach and the trimethyl phosphine were used in the latter case. Therefore, we performed additional full-QM calculations for the Grubbs catalyst with a $-Ph(i\text{-}Pr)_2$ imine substituent and the triphenyl phosphine, i.e., for the system directly corresponding to **1b′**. For this system we obtained the phosphine dissociation energy of 29.2 kcal/mol. Thus, it may be concluded that the results presented here support the experimental hypothesis[16] that the phosphine dissociation is much easier for the anilinotropone catalyst than for the salicylaldiminato system.

Relative Stability of Isomeric Alkyl Complexes. The relative energies for the isomeric propyl and butyl complexes with the generic and real catalyst are listed in the left column of Table 2. Three general trends may be observed by comparison of these energies: (i) comparing *cis*/*trans* isomers, the ones with the Me−C bond located in the position *trans* to the oxygen atom of the

(45) Chan, M. S. W.; Deng, L.; Ziegler, T. *Organometallics* **2000**, *19*, 2741.

catalyst are more stable; the *cis*/*trans* effect observed here is similar to that observed for the Grubbs salicylamidato catalyst;[45] (ii) the more branched the alkyl is, the more stable the corresponding β-agostic complex; (iii) the steric bulk on the real catalyst has little effect on the relative stability of the alkyl complexes.

There are two opposing factors determining the stability of alkyl complexes: (i) stability of free alkyl radicals, increasing for more branched systems; (ii) energy of binding of the radicals, decreasing for more branched alkyls. As a result, the energy order of isomeric alkyl complexes resembles the energy order of the alkyl radicals, with smaller energy differences between them than between the free radicals. A similar effect was observed for the Pd-diimine catalyst; in previous studies[20,21] we analyzed and discussed this in a more detailed way.

As for the diimine catalysts,[20,21] an increase of the steric bulk on the diimine nitrogens will slightly increase the energy difference between the *n*- and *iso*-Pr complexes [cf. E(**2′b-O**) vs E(**2b-O**) and E(**2′b-N**) − E(**2′c-N**) vs E(**2b-N**) − E(**2c-N**)]. As we argued for the Pd-diimine catalyst, this effect comes as a result of a (slightly) decreased bonding energy of the alkyl radical in the case of the real complexes.

It is also worth mentioning that in the real complexes the difference between the *cis*/*trans* isomers is slightly decreased compared to the systems with the generic catalyst. This is not surprising since one can expect a relatively large steric repulsion between alkyl and bulky imine substituents in the complexes **2′b-O**/**2′c-O** (alkyl *cis* to N and its substituent) compared to **2′b-N**/**2′c-N** (alkyl *trans* to N and its substituent).

Relative Stability of Ethylene π-Complexes with Different Alkyls. The relative energies of the isomeric ethylene π-complexes are listed in the right column of Table 2. In the π-complex geometries the repulsion between the olefin and the alkyl chain destabilizes the complexes with branched alkyls. Thus, for the generic catalyst the ethylene π-complexes with the linear butyl group (**3d-O**, **3d-N**) are the most stable, while the systems with the *tert*-Bu (**3h-O**, **3h-N**) have higher energy for both *cis*/*trans* isomers. For the propyl complexes the effect is obviously less pronounced, and the systems with *iso*-Pr remain slightly preferred. Again, the effect is qualitatively similar to that observed in the case of diimine catalysts.[20,21]

In the real systems the steric effect is substantially different for the *cis*/*trans* isomers. In the geometries with alkyl positioned *trans* to O, the repulsion between alkyl and catalyst substituent strongly destabilizes the branched isomer (**3′c-O**), and thus, the *n*-Pr complex (**3′b-O**) has a lower energy by ca. 4.5 kcal/mol. For N-*trans* complexes this steric effect is negligible and the *i*-Pr system (**3′c-N**) remains more stable by 0.9 kcal/mol than its *n*-Pr isomer. Since both O-*trans* complexes are destabilized for the real catalyst, the system **3c′-N** has the lowest energy among the four complexes.

We would like to emphasize at this point that the relative stabilities of the alkyl agostic and olefin π-complexes are important for the control of polyolefin branching. The stability of alkyls always shifts the equilibrium toward formation of branched chains, while the stability of π-complexes acts in the opposite directions for the two *cis*/*trans* isomers. Thus, both factors must be taken into account in predicting/modeling the polymer branching.[19−21] We will address this problem in the last section of this account.

Table 3. Ethylene Complexation Energies and the Insertion Barriers

	relative energy[a]							
	ethylene π-complexes[b]				insertion TS[b]			
alkyl	O-*trans*		N-*trans*		O-*trans*		N-*trans*	
Model Catalyst								
n-Pr	**3b-O**	−21.48	**3b−N**	−20.57	**4b-O**	27.24	**4b-N**	17.69
iso-Pr	**3c-O**	−20.64	**3c−N**	−20.20	**4c-O**	28.38	**4c-N**	18.64
Real Catalyst								
n-Pr	**3′b-O**	−18.76	**3′b-n**	−20.50	**4′b-O**	23.10	**4′b-N**	18.74
iso-Pr	**3′c-O**	−12.91	**3′c-N**	−19.84	**4′c-O**		**4′c-N**	19.88

[a] In kcal/mol. [b] See Scheme 2.

Ethylene Complexation Energies and the Insertion Barriers. The ethylene π-complexation energies and the insertion barriers are collected in Table 3. The energy profile for the polymerization cycle is shown in Figure 3.

The complexation energies of Table 3 reflect the effects of the relative stabilities of alkyl and olefin-alkyl complexes discussed in the previous paragraphs. For both catalysts, the complexation energies are slightly larger for the systems with a *n*-propyl group than for those with *i*-Pr. For the generic catalyst the formation of the ethylene π-complexes is more exotermic for the O-*trans* isomers than for the N-*trans* systems. For the real catalyst, however, the O-*trans* complexes are strongly destabilized, while the N-*trans* complexation energies are hardly affected by the steric effect. The destabilization of the olefin π-complex is especially pronounced for the system **3′c-O**, with an *i*-Pr group located close to the −Ph(*i*-Pr)$_2$ catalyst substituent.

It should be pointed out that the absolute values of the complexation energies for the generic catalyst (20−21.5 kcal/mol) are much larger than the corresponding values obtained for the Grubbs catalyst (17−18 kcal/mol).[45] For the real catalyst, however, the destabilization of the O-*trans* π-complexes is larger than for the related Grubbs system, for which the steric effect was found to be negligible.[45] It may be partially attributed to the difference in the size of the front ring (five-member vs six-member). However, it should be noticed also that for the Grubbs catalyst the less-sensitive QM-MM method was used[45] to estimate the steric effects, while in the present studies the full-QM approach has been applied.

As a result of higher stabilization of the ethylene π-complexes with the present catalyst compared to those for the Grubbs catalyst, the insertion barriers are higher here by ca. 2 kcal/mol. However, the same *cis*/*trans* effect can be observed for both catalysts. Namely, the insertion staring from the (less stable) **3b-N** isomer has a barrier lower by ca. 10 kcal/mol than the insertion starting from the (more stable) **3b-O** complex. As was argued for the Grubbs catalyst,[45] the high barrier in the case of the O-*trans* system comes as a result of the stabilization of the **3b-O** complex and a destabilization of the corresponding **4b-O** TS. For the real catalyst the difference between the two insertion barriers (**4b′-O**, **4b′-N**) is decreased to ca. 4.4 kcal/mol, but is still pronounced. It should be emphasized here that the

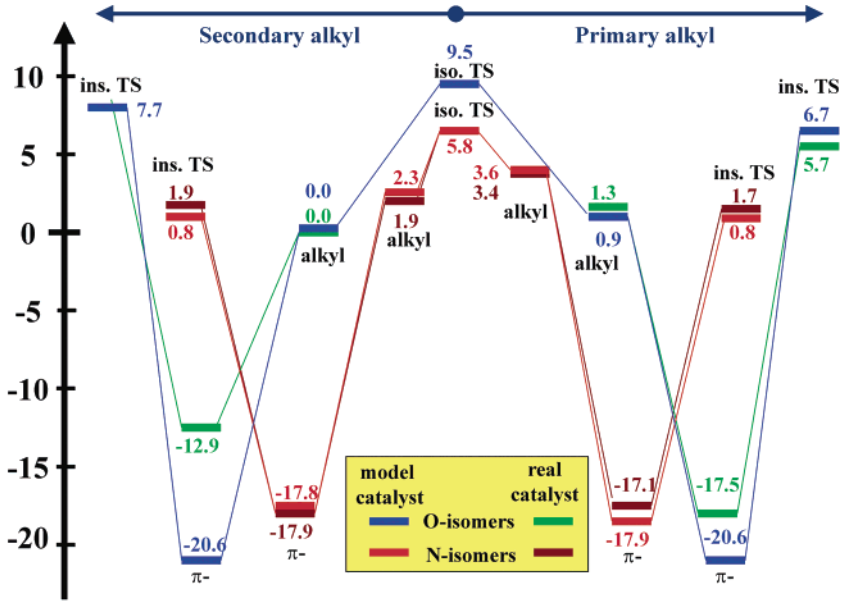

Figure 3. Energy profiles for the isomerization reactions and the ethylene insertion into the Ni−carbon bond involving primary (right) and secondary (left) carbon calculated for the model (blue and red) and real catalysts (green and brown, for O- and N-pathways, respectively).

Table 4. Relative Energies for the Stationary Points in the Isomerization Reactions

reaction[a] 2x → 2y		relative energy[b]				
x	y	**2x**	**TS (2x/2y)**	**5(x/y)**	**TS (y/x)**	**2y**
		Primary Alkyl → Secondary Alkyl				
d-O	**g-O**	0.00 (0.77)	8.01 (8.78)	6.97 (7.77)	8.77 (9.54)	−0.77 (0.00)
d-N	**g-N**	0.00 (0.73)	2.35 (3.08)	−1.66 (−0.96)	2.70 (3.43)	−0.73 (0.00)
		Primary Alkyl → Tertiary Alkyl				
e-O	**h-O**	0.00 (2.05)	7.71 (9.76)	5.96 (8.01)	6.91 (8.96)	−2.05 (0.00)
e-N	**h-N**	0.00 (2.61)	1.84 (4.45)	−2.90 (−0.33)	0.33 (2.94)	−2.61 (0.00)
		Secondary Alkyl → Secondary Alkyl				
f-O	**f-O**	0.00	6.23	5.44	6.23	0.00
f-N	**f-N**	0.00	4.11	2.52	4.11	0.00

[a] See Scheme 2. [b] With respect to the reactant (product), in kcal/mol.

"easier" insertions starting from the N-*trans* (**3b-N/3′b-N)** complexes result in the more stable O-*trans* alkyl and π-complexes, which give rise to a "difficult" insertion. Thus, the two pathways must alternate during the course of the polymerization process via the *cis*/*trans* isomerization of the alkyl or ethylene π-complexes. It has been found[45] for the Grubbs catalyst that such an isomerization between the two π-complexes has a barrier of ca. 11 kcal/mol. Since it is substantially lower than the insertion barriers, we did not study such isomerizations here; without any effect on the considerations presented in this article, it can be neglected (or considered as a part of the insertion barriers).

Finally, we would like to point out that the absolute TS energies for "primary" and "secondary" insertions are almost identical for the N-*trans* isomers (see Figure 3). Thus, for "primary" insertions the TS energies are noticeably lower than the energies of the mother alkyl complexes even for the real catalyst.

Chain Isomerization Reactions. The relative energies for the stationary points in the chain isomerization reactions are listed in Table 4; the simplified (with the highest energy TS only) isomerization energy profiles are also included in Figure 3. The results clearly show that the isomerization barriers (calculated relative to the alkyl complex energies) are much lower than those for the ethylene insertion (calculated with respect to the ethylene π-complexes). However, the absolute energies for the isomerization TS are higher than those for the insertion TS (see Figure 3).

It should be noticed also that in all the cases the isomerization starting from the higher energy *cis*/*trans* isomer has a substantially lower barrier. In the case of the "primary → secondary alkyl" isomerizations, the pathway starting from **2d-O** has a barrier of 9.5 kcal/mol (**TS 2g/2d-O**), while the TS for the alternative pathway (**TS 2g/2d-N)** that starts from **2d-N** is located only 3.4 kcal/mol above the initial alkyl complex **2d-N**. Similarly, for the "primary → tertiary alkyl" isomerization the two highest TS have energies of 7.7 kcal mol (**TS 2e/2h-O**) and 1.8 kcal/mol (**TS 2e/2h-N**), respectively; for the "secondary → secondary alkyl" the barriers are 6.2 kcal/mol (**TS 2f/2f-O**) and 4.1 kcal/mol (**TS 2f/2f-N**), respectively. Thus, it may be concluded that for this catalyst the **-N** isomers (with alkyl *trans* to the catalyst's N atom) are the active species in the case of both ethylene insertion and chain isomerization reactions (see also Figure 3).

The results of Table 4 also show that in all cases the olefin-hydride complexes (**5x/y**) resulting from the β-hydrogen abstraction form stable minima on the potential energy surfaces with energies that are lower by 1−5

Table 5. Relative Energies for Methyl Acrylate Complexes

relative energies[a]			
acrylate π-complex[b]		acrylate O-complex[b]	
Model Catalyst			
9b-O	0.00 (−19.51)	**10b-O**	8.50 (−8.41)
9b-N	1.87 (−20.43)	**9b-N**	13.84 (−11.00)
Real Catalyst			
9′b-O	1.00 (−17.60)	**10′b-O**	8.81 (−8.97)
9′b-N	0.00 (−18.75)	**10′b-N**	8.60 (−10.94)

[a] With respect to the most stable isomer; complexation energies in parantheses; in kcal/mol. [b] See Scheme 2.

kcal/mol than those of the corresponding transition states (**TS 2x/2y** and **TS 2y/2x; x/y** = {**d/g, e/h, f/f**}). The hydride-olefin complexes are especially stable for the **-N** pathways (with alkyl *trans* to N): the complexes **5d/g-N** and **5e/h-N** are even lower in energy than the starting/final alkyl β-agostic complexes **2d-N**, **2g-N** and **2e-N, 2h-N**, respectively. This comes as a result of stabilization of the olefin resulting from the hydride abstraction by the catalyst nitrogen atom located in the *trans* position. The same factor determines the stability of the olefin π-complexes discussed previously; we would like to recall at this point that the complexes **3x-O** with the olefin in the position *trans* to N are more stable than the **3x-N** isomers (**x** = **b**−**h**).

The low isomerization barriers underline the fact that the Ni-anilinotropone catalyst can produce branched polyethylenes under certain reaction conditions and that the degree of branching can be controlled by the thermodynamic parameters of the process (temperature and pressure) as observed experimentally.[16] In the last part of this account we shall discuss this in detail on the basis of the results of stochastic simulations of the polyethylene growth in the processes catalyzed by this complex.

Functional Group Tolerance: Methyl Acrylate Binding. The relative stabilities of the methyl acrylate complexes together with the complexation energies are listed in Table 5. The results demonstrate that for both the generic and real catalysts the complexes in which the polar monomer is bound by its olefinic functionality are substantially more stable (by 7.6−12 kcal/mol) than the complexes with the acrylate bound by its carbonyl oxygen. For both binding modes the **-O** *cis*/*trans* isomers (with alkyl *trans* to O) have lower energies than the **-N** complexes. A destabilization of the **-N** isomer is especially pronounced in the case of the complex **9b-N**, in which the two oxygen atoms (catalyst's and monomer's) are positioned *trans* to each other; this complex is higher in energy by 5.3 kcal/mol than the other *cis*/*trans* isomer **9b-O**.

For the generic catalyst the lowest energy π-complex of methyl acrylate (**9b-O)** is more stable than the oxygen-bound complex (**10b-O)** by 8.5 kcal/mol. This difference is larger than the corresponding value for the Grubbs catalyst (7.6 kcal/mol).[24] For the real complexes the difference in the two energies (**9′b-O** vs **10′b-O**) increases slightly for the catalyst investigated here (to 8.8 kcal/mol), whereas for the Grubbs real catalyst it was found to be smaller (6.3 kcal/mol).[24] These results clearly demonstrate that the Ni-anilinotropone complex should be even more functional group tolerant than the Ni-salicylamidato complex. This conclusion supports the experimental observations that this catalyst is almost insensitive for polar additives.[16]

Finally, we would like to discuss the complexation energies for the two binding modes of methyl acrylate. The complexation energies reflect the stability trends for both the acrylate complexes and the mother alkyl complexes. Since the energy difference between the two *cis*/*trans* isomers is larger for the alkyl agostic complexes (**2b-O** vs **2b-N**) than for the acrylate π-complexes (**9b-O** vs **9b-N**), it is not surprising that the complexation energy is larger for the higher energy complex **9b-N** (−20.4 kcal/mol) than for **9b-O** (−19.5 kcal/mol); the same is true for the oxygen-bound complexes as well for the systems involving the real catalyst.

The complexation energies for the acrylate π-complexes with the real catalyst are smaller by ca. 2 kcal/mol than for the systems with the model catalyst. This decrease in the π-complex stabilization is much smaller than for the corresponding effect for the salicylamidato catalysts (decrease by ca. 5 kcal/mol; from −17.7 kcal/mol to −12.8 kcal/mol).[24] As a result, the acrylate π-complexation energy for the complex **9′b-O** with the real anilinotropone catalyst is smaller than the corresponding ethylene complexation energy (**3′b-O**, see Table 3) by only 1.2 kcal/mol. For the real Grubbs catalyst the complexation energy for acrylate (−12.8 kcal/mol)[24] was found to be substantially smaller than for ethylene (−16 to −18 kcal/mol).[21] This result may indicate that the catalyst studied here may be a good candidate for the copolymerization of ethylene with polar monomers. It has been found experimentally[5] and theoretically[46] that the low incorporation of polar monomer in the copolymerization catalyzed by the diimine catalyst comes as a result of weaker acrylate bonding, whereas the acrylate insertion barriers in are fact lower than the ethylene insertion barriers. Thus, the anilinotropone catalyst, if capable of copolymerizing the polar monomers, should lead to a higher incorporation of functionalized monomer. Certainly, on the basis of the studies of acrylate binding only, it is not possible to predict the copolymerization activity; for this, detailed mechanistic studies are required involving evaluation of the barriers for polar monomer instertion and the opening of the chelates formed during copolymerization process. This is certainly beyond the scope of this article.

Pressure and Temperature Dependence of Polyethylene Branching/Microstructure. As we have already argued on the basis of the results of the DFT calculations, the degree of branching and the topology of the polyolefins produced by any catalyst is controlled by various factors, often opposing each other, such as relative stabilities of the isomeric, linear, and branched alkyl complexes, relative stability of the isomeric ethylene π-complexes, relative insertion barriers for the "primary" and "secondary" insertions, and the barriers for all alternative isomerization reactions. Thus, it is not possible to directly predict the number of branches from the calculated energetics and especially the topology of resulting polymer. Therefore, to model the microstructure polymer, we employed a stochastic model introduced recently.[19] Such an approach allows us to model the temperature and pressure dependence of the

(46) Michalak, A.; Ziegler, T. *J. Am. Chem. Soc.* **2001**, *123*, 12266.

polymer microstructure based on the calculated energies of the elementary reactions and their activation barriers.

For the catalyst studied in the present article, all the reaction pathways are "doubled", due to *cis*/*trans* isomerization. However, the results of the DFT calculations demonstrate that the "active" pathways of both chain propagation and isomerization reactions do not start from the most stable species, but from the higher energy complexes with alkyl located *trans* to the N atom on the catalyst. Therefore, as data for the simulations we used the relative energies of the species present in those **-N** pathways. We do not take into account the formation of the **-O** species, nor the *cis*/*trans* isomerization events, that would only slow the simulation without any effect on the polymer microstructure. The *cis*/*trans* isomerization is required for the polymerization process to proceed though, since the insertions from **-N** species produce **-O** isomers (Scheme 3). However, as long as the *cis*/*trans* isomerization barriers are lower than that of ethylene insertions, they can be neglected (considered as a part of the insertion barrier). Thus, as the data for the present stochastic simulations we used the energies of the **-N** species calculated for the real catalyst.

The details of the model employed have been presented in our recent study[19] and are briefly summarized in the Computational Details section. Thus, we would not like to repeat them here. However, we would like to point out that the temperature dependence is modeled by the T parameter with the *real* temperature values. For the pressure parameter p an *arbitrary* unit is used, so its values do not correspond directly to the "real" polymerization pressure, $P = sp$. The scaling parameter s ("unit conversion") depends on various factors characterizing the real polymerization condition, e.g., ethylene solubility in a given solvent. The theoretical estimation of the scaling factor s is given in the Appendix.

In the Brookhart studies[16] the polymerization experiments were performed for $T = 40-100$ °C (at $P = 400$ psig) and $P = 14-600$ psig (at $T = 80$ °C). To model the topology of the polymer under different temperature and pressure conditions and to relate our results to the experimental data, we first performed a set of simulations for $T = 80$ °C and the wide range of the pressure parameter $p = 10^{-6}-1$. The results are presented in Figure 4a. The number of branches/1000 C changes from zero at $p = 1$ to ca. 200 at $p = 10^{-4}$ and remains constant for lower p values. Under the experimental conditions the number of branches vary between 41 at $P = 600$ psig and 113 branches/1000 C for $P = 14$ psig. By comparison of the experimental data (61 branches/1000 C at $P = 200$ psig)[16] and the results of our simulations (61 branches/1000 C at $p = 0.0076$) we are able to identify the experimental range of pressures in our plot and find the "unit conversion" parameter $s = 2.632 \times 10^4$. This value is relatively close to our rough estimate of s presented in the Appendix. We would like to emphasize here that there has been no empirical fitting performed in order to determine the curves presented in Figure 4a,b; the simulations have been performed on the basis of the energetics of the elementary reactions obtained from the first-principles (DFT) calculations presented above. The pressure scaling ("unit conversion") is required only to compare the theoretical and experimental curves.

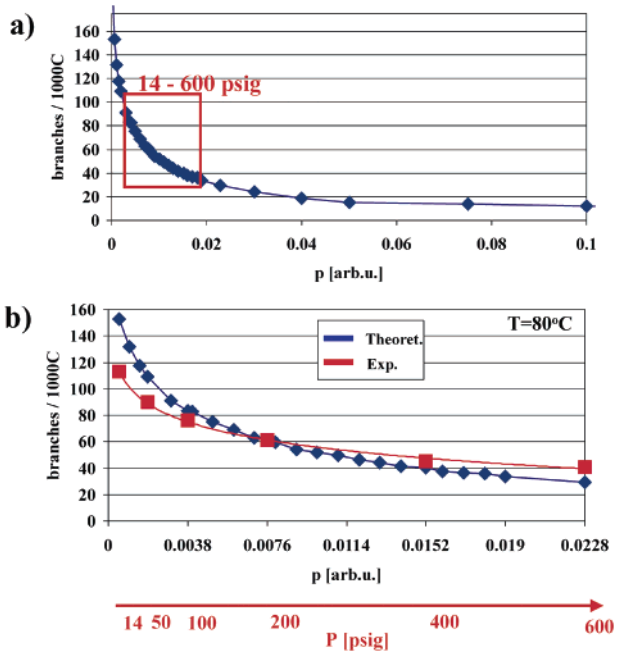

Figure 4. Calculated (blue) and experimental (red) pressure dependence of the average no. of branches/1000 C. Panel a presents results of the simulations for $p = 10^{-6}-10°$, while the results of the simulations corresponding to the experimental range of pressure ($P = 14-600$ psig, $p = 0.00053-0.0228$, see text) are magnified in panel b.

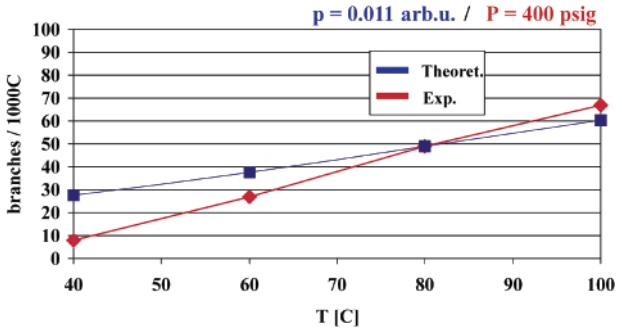

Figure 5. Calculated (blue) and experimental (red) temperature dependence of the average no. of branches/1000 C from the simulations at $T = 40-100$ °C and $P = 400$ psig ($p = 0.015$, see text).

The results obtained in the experimental range of pressure ($P = 14-600$ psig, $p = 0.00053-0.00228$) are magnified in Figure 4b. Taking into account the simplicity of our model and the accuracy of experimental results (±5−10 branches/1000 C), the agreement between the experiment and theory is very good. The theoretical curve is slightly steeper than the experimental one. At $P = 600$ psig ($p = 0.0228$) the theoretical value of 30 branches/1000 C is slightly underestimated (expt 41 branches/1000 C), and at $P = 14$ psig ($p = 0.00053$) the value of 153 branches/1000 C obtained from the simulations is noticeably larger than the experimental result (113 branches/1000 C). This difference may be due to neglecting the entropic contributions to the barriers of elementary reactions and the solvent effects in our simulations.

Table 6. Influence of the Reaction Conditions (*T*, *p*) on the Polymer Topology

reaction conditions		branches/ 1000 C	% of C atoms in main chain	% of C atoms in primary branches	% of C atoms in secondary branches	av (max.) length of primary branches	av (max.) length of secondary branches	av (max.) length of tertiary branches
T [°C]	*P* [psig]							
40	400	21.0	97.7	2.3	0.0	1.1 (4)	0.0 (0)	0.0 (0)
60	400	29.8	96.7	3.3	0.0	1.2 (4)	0.0 (1)	0.0 (0)
80	400	39.7	95.4	4.6	0.0	1.2 (5)	0.0 (1)	0.0 (0)
100	400	50.1	94.0	6.0	0.0	1.2 (7)	0.0 (2)	0.0 (0)
80	14	153.5	59.4	35.0	2.1	2.7 (23)	2.1 (10)	1.2 (7)
80	50	108.4	81.0	18.0	1.0	1.8 (11)	1.1 (4)	0.0 (1)
80	100	83.0	87.9	12.0	0.1	1.46 (8)	0.85 (2)	0.0 (0)
80	200	60.9	92.2	7.8	0.0	1.28 (6)	0.0 (1)	0.0 (0)
80	600	30.0	96.7	3.3	0.0	1.1 (4)	0.0 (0)	0.0 (0)

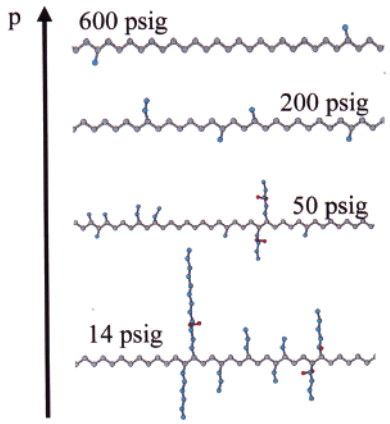

Figure 6. Examples of the polyethylene structures obtained from the simulations with different olefin pressure ($P = 14-600$ psig, $T = 80$ °C). Different colors are used to mark different types of branches (primary, secondary, etc.).

The temperature dependence of the number of branches is presented in Figure 5. This curve has been obtained from the set of simulations performed at $p = 0.015$ ($P = 400$ psig) for $T = 40-100$ °C. In agreement with experiment,[16] the stochastic simulations predict an increase with the number of branches with an increase in *T*. This comes as a result of an increase in the number of the "secondary" insertions with temperature. As the energy profile of Figure 3 shows, the TS for the secondary insertion has a higher energy than the "primary" insertion TS, while the initial "secondary" β-agostic complex is more stable. Thus, the probability of the secondary insertions (introducing new branches) increases with temperature. The slopes of the experimental and theoretical curves are slightly different. The disagreement is slightly larger for low temperatures: at $T = 40$ °C the simulations give 21 branches/1000 C, while the experimental value is 8 branches/1000 C, and at $T = 100$ °C the theoretical prediction is slightly underestimated (52 branches/1000 C vs 67 branches/1000 C). However, the overall agreement is reasonable.

Finally, we would like to discuss the temperature and pressure influence on the polymer topology. The examples of the polyolefin structures obtained from the simulations under different conditions are presented in Figure 6. The quantitative structural characteristics of the polymers are listed in Table 6. Let us first discuss the pressure dependence. At $P = 600$ psig 97% of the atoms are located in the main polymer chain, the remaining 3% in the methyl branches. At $P = 14$ psig, 35% of atoms are located in the primary branches (starting from the main chain), 2% in the secondary branches (starting from the primary branches). The average length of the primary branches is 2.7 carbon atoms. However, much longer (up to 23 carbons) primary branches occur sporadically. The average length of the secondary branches is 2.1 carbon atoms; the longest produced secondary branch has 10 carbon atoms. Sporadically, the tertiary branches are formed (0.21% of atoms, i.e., ca. 2 tertiary branches/10000 C); the longest observed tertiary branch has 7 carbons.

It can be concluded that the pressure change has a much stronger effect on the polymer topology than the temperature. At $T = 40$ °C 97.9% of atoms are located in the main polymer chain, the rest in methyl branches. At $T = 100$ °C the percentage of atoms in the main chain decreases only slightly (to 93.9%), 6% are located in the primary branches (average length: 1.2 C, longest: 7 C), and only 0.01% in the secondary branches.

Thus, the results presented here demonstrate that the polymer topology may be controlled to some extent by a variation in the polymerization pressure. Further, changes in the polymerization temperature can modify the number of branches, without a strong influence on the polymer topology. Similar pressure/temperature effects were observed for the diimine-based catalysts. For the catalyst studied in the present work, no experimental characterization of the polymer topology has been published yet.

Concluding Remarks

We have performed a detailed DFT study on the mechanism of ethylene polymerization catalyzed by a neutral Ni-anilinotropone catalyst; the generation of active species by the phosphine dissociation, as well as the chain propagation and chain isomerization reactions, have been investigated. We have also addressed the issue of prospective polar copolymerization by analyzing the alternative methyl acrylate binding modes. Further, we have used DFT-calculated energetics of the elementary reactions to model the influence of the reaction conditions (*T*, *P*) on the branching/microstructure of polyethylenes produced in this process.

The results of the calculations for the phosphine dissociation reaction indicate that for the model (generic) catalyst the enthalpy of the reaction is higher than for the analogous salicylamidato catalyst, while for the real catalyst this reaction is less endothermic than for the Grubbs systems. This supports the experimental results.[16]

The results of DFT calculations for the isomeric alkyl agostic complexes indicate the energetic preference of the branched alkyl complexes. However, the ethylene

π-complexes with linear alkyl are more stable than the branched species. Thus, the stability of the alkyl complexes shifts the equilibrium toward formation of the branched species, while the stability of the ethylene complexes favors the formation of linear structures. The stability trends are similar to those previously reported for diimine catalysts.[20,21]

The DFT results clearly demonstrate that the energetically preferred pathways for both the chain propagation and chain isomerization reactions start for the higher energy *cis*/*trans* isomers. For the generic catalyst, barriers for the ethylene insertion pathways starting from the less stable **-N** isomers (with alkyl positioned *trans* to the N atom on the catalyst*)* are lower by ca. 10 kcal/mol than those starting from the most stable **-O** isomers. For the real complexes the difference in the activation barriers for the two isomeric pathways are lowered, but are still substantial. This is similar to the case of the Grubbs catalyst.[45] In the case of the isomerization reactions, the **-N** pathways have very low barriers (2.4−4.5 kcal/mol for different alkyl species). Along these pathways, the unusually stable olefin-hydride complexes are formed, some of them being more stable (by 1.5−3 kcal/mol) than the alkyl agostic complexes.

The results of the calculations for the methyl acrylate complexes confirm the high tolerance of the anilinotropone catalyst toward polar groups.[16] The π-complexes are more stable by 8−13 kcal/mol than the systems with the acrylate molecule bound by its carbonyl oxygen. This functional group tolerance is larger than for the Grubbs catalyst.[24] The calculations also indicate that the acrylate π-complexation energies are less affected by the steric bulk than in the case of salicylamidato catalysts and the diimine catalysts.[24] This suggests that if this catalyst is capable of copolymerizing the polar monomers with ethylene, it should lead to larger comonomer incorporation than that of Pd-diimine complexes.

Finally, the results from the stochastic simulations of the polymer growth reproduce the experimentally observed[16] dependence of the average number of branches on temperature and pressure. In addition, the stochastic simulations provided detailed information about the topology of the polyethylenes produced in these processes. The results indicate that a variation in pressure affects the polymer topology more than a variation in temperature. At the low-pressure regime the length of the branches increases and the branch-on-branch structures are formed more often.

The optimized geometries of the discussed structures and any further computational details are available from the authors upon request.

Acknowledgment. This work has been supported by the National Sciences and Engineering Research Council of Canada (NSERC) as well as donors of the Petroleum Research Fund, administered by the American Chemical Society (ACS-PRF No. 36543-AC3). A.M. acknowledges the NATO Postdoctoral Fellowship. T.Z. thanks the Government of Canada for a Canada Research Chair.

Appendix

In the stochastic simulations, for the pressure parameter p an *arbitrary* unit is used, so its values do not correspond directly to the "real" polymerization pressure, $P = sp$. The question that naturally arises, is whether it is possible to estimate the s value from "first principles". It should be emphasized here that we intend to use the calculated *gas phase energies* as data for the simulations, and not *the free energies in solution*. Thus, there are three major factors influencing the scaling of p, compared to the real pressure P: (i) the entropic part of the ethylene complexation free energies, affecting the complexation equilibrium constant, K, and thus, the relative isomerization/insertion probabilities, $\pi_{iso}/\pi_{ins} = k_{iso}/(k_{ins}Kp)$, where k_{iso} and k_{ins} are the insertion and the isomerization rate constants; we discussed this in a more detail in a previous work;[19] (ii) a difference between the gas phase free energies and those in solution, again affecting K; (iii) the solubility of ethylene in a given solvent and its pressure dependence.

The gas phase entropy of olefin complexation varies between 27 and 36 eu,[5] which corresponds to $-T\Delta S =$ ca. 9−12 kcal/mol at room temperature. For the catalyst studied here we obtained the value of $-T\Delta S = 12.5$ kcal/mol from the frequency calculations. Let us now discuss the possible solvation effect on the entropies of the ethylene complexation reaction, **2** + C_2H_4 → **3**. It can be expected that the difference between the reaction entropy in solution $\Delta S_s = S_s(\mathbf{3}) - S_s(\mathbf{2}) - S_s(C_2H_4)$ and the gas phase entropy $\Delta S_g = S_g(\mathbf{3}) - S_g(\mathbf{2}) - S_g(C_2H_4)$ is mainly due to the ethylene solvation $\Delta S_s - \Delta S_g \approx S_g(C_2H_4) - S_s(C_2H_4)$, since the solvation entropies of complexes **2** and **3** should be similar, $S_s(\mathbf{3}) - S_g(\mathbf{3}) \approx S_s(\mathbf{2}) - S_g(\mathbf{2})$. The ethylene solvation entropy in typical solvents used in polymerization processes is ca. 16 eu.[47] Thus, the entropic contribution to the free energy of ethylene complexation in solution will be lower by ca. 5 kcal/mol, to give $-T\Delta S = 7.5$ kcal/mol in solution. This gives an order of magnitude of the conversion factor $s = \Delta K = \exp(-\Delta S/R) \approx 10^5$. The solubility of ethylene is ca. 0.2 mol L^{-1} atm^{-1},[5] so this factor introduces much smaller correction compared to (i) and (ii). Thus, the estimated value of the scaling parameter s would be ca. 5×10^5 when the pressure unit is atm and ca. 3.5×10^4 when the pressure is expressed in psig. We would like to emphasize here that this is a rough estimate that gives only an order of magnitude accuracy. However, it should be emphasized that this estimation agrees quite well with the value found by comparison of the theoretical and experimental pressure dependence of the olefin branching number ($s = 2.632 \times 10^4$; see text).

To be able to model the "real" pressure values directly from the quantum chemical calculations, one would need the accurate free energies of elementary reactions in a givent solvent and the pressure dependence of the ethylene solubility. This is certainly beyond the quantum chemical modeling at the moment.

OM030072+

(47) Wilhelm, E.; Battino, R *Chem. Rev.* **1973**, *73*, 1.